ACOUSTIC PREDICTION OF HELICOPTER UNSTEADY MANOEUVRES

Massimo Gennaretti[§], Giovanni Bernardini[§], Jacopo Serafini[§]
Lorenzo Trainelli[¶], Alberto Rolando[¶],
Alessandro Scandroglio[*], Luca Riviello[*], Enrico Paolone[*]

[§]Department of Engineering, Roma Tre University, Rome, Italy
[¶]Department of Aerospace Science and Technology, Politecnico di Milano, Milano, Italy
[*]AgustaWestland, Cascina Costa, Italy

Abstract

Real-time estimation techniques of helicopter noise in manoeuvring flight are examined. They consist of quasi-steady aeroacoustic predictions based on noise-sources (given in terms of hemispheric acoustic maps rigidly connected to the rotorcraft) suitably extracted from a database generated through off-line aeroacoustic analysis of rectilinear, steady-state flights. This is of interest for the Clean Sky GRC5 MANOEUVRES project, which aims at developing an in-flight noise monitoring system to make the pilot aware of acoustic disturbance produced. Considering a helicopter in an approach manoeuvre, the accuracy of the quasi-steady acoustic approaches is assessed by comparison with fully unsteady simulations, and the sensitivity of their predictions on the quality of the estimation of the flight parameters considered to extract the suitable instantaneous hemispheric acoustic maps from the database is examined.

1. INTRODUCTION

Accurate prediction of noise generated aerodynamically by helicopters represents nowadays a critical issue for research and development of modern rotorcraft. Indeed, capability of accurate evaluation of the sound field emitted in arbitrary manoeuvres plays a fundamental role in estimating acoustic impact and detectability of the noise source, as well as in developing tools suitable for studying noise reduction techniques. Among the several strategies examined for noise alleviation purposes, in the last decade, the identification of minimum-noise, optimal trajectories has been widely applied,[1–3] in that providing effective solutions without requiring specific machine adaptation (*i.e.,* re-design or retrofit solutions). This methodology often combines a flight simulation model, a near-field noise model, a far-field noise propagation model and geographic information to make optimization suitable for orography and population density distribution of the interested area. Identified minimum noise trajectories might correspond to unsteady manoeuvres including turns, varying flight-path slope, accelerations and decelerations, which require acoustic source model update accordingly to the change of flight conditions. In order to avoid numerically expensive acoustic predictions, this is usually accomplished by deriving the near-field model (provided in terms of a hemispheric acoustic map rigidly con-

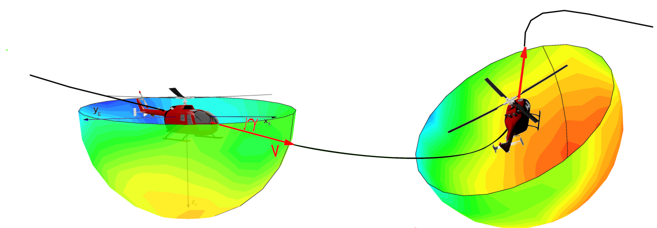

Figure 1: Noise hemisphere concept.

nected to the rotorcraft, see Fig. 1) from an appropriate database generated through off-line aeroacoustic analysis of rectilinear steady-state flights, related to a number of points within a given domain of flight parameters suitably characterizing the noise source state (quasi-steady acoustic approach).

Similar aeroacoustic information is required for the activities of the Clean Sky GRC5 MANOEUVRES project.[4,5] Indeed, it includes the development of a helicopter in-flight noise monitoring system (the Pilot Acoustic Indicator - PAI) designed to enhance pilot's noise awareness and allow him/her to react adequately in case of exceeding admissible acoustic disturbance.[6] The PAI relies on a noise estimation algorithm which determines in real-time, a suitable measure of the acoustic impact by interpolating the hemispheric acoustic map within the database, as a function of current values of helicopter advance ratio, main rotor thrust coefficient, and main rotor tip-path-plane angle of attack (TPP-AOA).

The aim of this work is twofold: (i) assessment of the accuracy of noise predictions based on quasi-steady acoustic approaches with respect to those given by fully unsteady simulations, and (ii) analysis of sensitivity of quasi-steady acoustic predictions on the accuracy of the estimation of the three parameters (namely, advance ratio, thrust coefficient, and TPP-AOA) used to extract the suitable instantaneous hemispheric acoustic map from the database. The attention is focussed on the acoustic disturbance radiated by the main rotor.

In the fully unsteady approach (indicated as *technique A*) all flight data, including pilot controls, helicopter attitude, rotor states and airloads, are provided by a rotorcraft aeromechanics simulation code coupled with a full-unstructured panel method solution tool for rotor aerodynamics.[7] Once spanwise distributed airloads are known, a compact-source aeroacoustic solver based on the Farassat Formulation 1A[8,9] is applied to determine the time history of the corresponding acoustic hemispheres, as evaluated by suited signal windowing.

Concerning the quasi-steady acoustic prediction, two approaches are investigated. The first (indicated as *technique C*) is inspired by a procedure considered in the MANOEUVRES project applicable in flight to feed the PAI, which is based on a simplified aeromechanical model of the rotorcraft to derive real-time estimates of advance ratio, thrust coefficient, and TPP-AOA. The second (indicated as *technique B*) represents a modification of the former, where the model-based estimation of the TPP-AOA is replaced by an evaluation process that exploits the availability of a main-rotor-state measurement system capable to track the motion of one or more blades. This novel measurement system is one of the main outcomes of project MANOEUVRES, and is currently in an advanced stage of development.[5] Note that, both techniques rely on an acoustic database determined by the compact-source aeroacoustic solver[8,9] applied to a series of rectilinear, steady-state flights associated to a finite number of operating conditions included in a suited domain of advance ratio, thrust coefficient, and TPP-AOA. Thus, the difference between the predictions provided by *technique B* and *technique C* highlights the sensitivity of quasi-steady simulations on the accuracy of rotor TPP-AOA estimation/measurement, which is one of the main objectives of project MANOEUVRES.

The following sections provide an outline of: (i) the compact-source aeroacoustic formulation applied for the steady-flight and unsteady-flight analyses, (ii) the aeromechanics solver used to simulate steady and manoeuvring helicopter flights, (iii) the aerodynamic tool providing blade loads starting from the flight conditions predicted by flight mechanics analyses. Finally, considering an intermediate weight helicopter performing an approach manoeuvre, aeroacoustic predictions derived from application of *technique B* and *technique C* are compared with those obtained from *technique A*, at some specific points of the trajectory, where unsteady effects inducing significant variations in inertial and aerodynamic loads occur. Particular attention is paid on the analysis of the sensitivity of quasi-steady acoustics predictions on the estimation of parameters characterizing the noise source identification.

2. NOISE PREDICTION TECHNIQUES

The noise prediction techniques examined in this paper require the sequential application of three solution tools: (i) an aeromechanics solver for the identification of the helicopter flight conditions corresponding to a given manoeuvre, (ii) a rotor aerodynamics solver that, for given flight conditions provides the associated blade airloads and finally, (iii) an aeroacoustic tool that determines the acoustic field generated by the rotor loads.

These tools are applied either to study as accurately as possible the noise emitted during an unsteady manoeuvre of the helicopter, or to generate a database of noise sources corresponding to a number of rectilinear, steady-flight conditions included in a domain of flight parameters suitably defined, to be exploited in the quasi-steady acoustic approaches.

The noise sources are given in terms of sound pressure levels evaluated on a hemispheric surface centred at the main rotor hub, fixed with the fuselage and with the equatorial plane parallel to the cabin floor. The flight parameters considered as those suited to characterize the helicopter acoustic emission pattern are the advance ratio, μ, the thrust coefficient, C_T, and the main rotor tip-path plane orientation with respect to relative wind, *i.e.,* the TPP-AOA, α_{TPP}.

Then, given an unsteady helicopter manoeuvre, the noise evaluation techniques considered in this work for the purposes mentioned in Section 1, are summarized as follows:

- *Technique A* – the aeromechanics tool provides corresponding time histories of pilot commands, centre of mass trajectory and velocity, helicopter orientation; for these flight conditions the aerodynamic tool yields rotor blade airloads which, in turn, are used in the aeroacoustic solver to evaluate the acoustic disturbance generated by the main rotor during the manoeuvre in terms of instantaneous noise hemispheres;

- *Technique B* – the time evolution of (μ, C_T, α_{TPP}) is determined from the aeromechanics tool predictions and then, the current values of these flight parameters at a discrete number of trajectory points are considered to extract the corresponding noise hemisphere from the noise database; this approach simulates the envisioned augmented in-flight procedure, with the data provided by the aeromechanics tool standing in for the on-board availability of inertial (accelerometer) and rotor state (blade flapping) measurements.

- *Technique C* – the noise hemispheres are extracted from the database considering the time evolution of (μ, C_T) determined from the aeromechanics tool predictions as above (*i.e.,* corresponding to the outcome of on-board measurements), and the α_{TPP} time history estimated by applying a simplified, real-time helicopter dynamics model; this approach simulates the in-flight procedure actually applicable due to the current unavailability of measurements of main rotor disc orientation with respect to the fuselage, and hence of TPP-AOA measure-based estimation in flight.

Aeroacoustics, aeromechanics and aerodynamics prediction tools applied in this work are described in the next sections.

3. AEROACOUSTIC SOLVER FOR ARBITRARY MANOEUVRING FLIGHT

Noise radiated by helicopter rotor blades is evaluated through solution of the well-known Ffowcs Williams and Hawkings equation,[10] which governs the propagation of acoustic disturbances aerodynamically generated by moving bodies.

The boundary integral formulation developed by Farassat known as Formulation 1A[9] is a widely-used, computationally efficient way to determine solutions of the Ffowcs Williams and Hawkings equation, and is particularly suited for the problems examined here. When the velocity of the rotor blades is far from the transonic/supersonic range, it yields the aeroacoustic field as a superposition of two terms, both expressed by integrals evaluated over the actual blade surface, S_B:[9] the loading noise, p'_L, related to the distribution of pressure over blade surfaces

$$
\begin{aligned}
(1)\qquad 4\pi p'_L(\mathbf{x},t) &= \frac{1}{c_0}\int_{S_B}\left[\frac{\dot{\tilde{p}}\,\mathbf{n}\cdot\hat{\mathbf{r}}+\tilde{p}\,\dot{\mathbf{n}}\cdot\hat{\mathbf{r}}}{r|1-M_r|^2}\right]_\tau \mathrm{d}S(\mathbf{y})\\
&+\int_{S_B}\left[\frac{\tilde{p}\,\mathbf{n}\cdot\hat{\mathbf{r}}-\tilde{p}\,\mathbf{M}\cdot\mathbf{n}}{r^2|1-M_r|^2}\right]_\tau \mathrm{d}S(\mathbf{y})\\
&+\frac{1}{c_0}\int_{S_B}\left[\frac{\tilde{p}\,\mathbf{n}\cdot\hat{\mathbf{r}}}{r^2|1-M_r|^3}\,r\dot{\mathbf{M}}\cdot\hat{\mathbf{r}}\right]_\tau \mathrm{d}S(\mathbf{y})\\
&+\int_{S_B}\left[\frac{\tilde{p}\,\mathbf{n}\cdot\hat{\mathbf{r}}}{r^2|1-M_r|^3}(M_r-M^2)\right]_\tau \mathrm{d}S(\mathbf{y})
\end{aligned}
$$

and the thickness noise, p'_T, that depends on blade geometry and kinematics

$$
\begin{aligned}
(2)\qquad 4\pi p'_T(\mathbf{x},t) &= \int_{S_B}\left[\frac{\rho_0\dot{v}_n}{r|1-M_r|^2}\right]_\tau \mathrm{d}S(\mathbf{y})\\
&+\int_{S_B}\left[\frac{\rho_0 v_n\left(r\dot{\mathbf{M}}\cdot\hat{\mathbf{r}}+c_0M_r-c_0M^2\right)}{r^2|1-M_r|^3}\right]_\tau \mathrm{d}S(\mathbf{y})
\end{aligned}
$$

In the equation above, $\mathbf{r}$ denotes the distance between observer position, $\mathbf{x}$, and source position, $\mathbf{y}$, whereas $\hat{\mathbf{r}}=\mathbf{r}/r$ is the unit vector along the source-observer direction, with $r=|\mathbf{r}|$. In addition, c_0 and ρ_0 are the speed of sound and the density in the undisturbed medium, respectively, $\tilde{p}=(p-p_0)$ with p_0 representing the undisturbed medium pressure, $\mathbf{M}=\mathbf{v}_B/c_0$ with $\mathbf{v}_B$ denoting the body velocity, $M=\|\mathbf{M}\|$, $M_r=\mathbf{M}\cdot\hat{\mathbf{r}}$, and $v_n=\mathbf{v}_B\cdot\mathbf{n}$, where $\mathbf{n}$ is the outward blade surface unit normal vector. Further, $\dot{v}_n$, $\dot{\mathbf{n}}$ and $\dot{\mathbf{M}}$ denote time derivatives of v_n, $\mathbf{n}$ and $\mathbf{M}$, observed in a frame of reference fixed with the undisturbed medium. The notation $[...]_\tau$ indicates that all quantities must be evaluated at the emission time τ, *i.e.,* the time at which the signal arriving in $\mathbf{x}$ at time t started from $\mathbf{y}\in S_B$.[9]

In problems dealing with weakly loaded rotors, thickness and loading noise are comparable. However, when strongly loaded rotors are examined, thickness noise contribution tends to be negligible and the acoustic disturbance is dominated by loading noise. Rotors in BVI conditions fall within this category of acoustic phenomena. Thus, from Eq. (1) it is apparent that for accurate noise simulation, accurate simulation of blade airloads is required.

Commonly, applications of aeroacoustic formulations for helicopter rotor analysis consider steady, rectilinear, trimmed flights. In these operative conditions both kinematics and aerodynamics are periodic thus yielding, correspondingly, periodic integrand functions, periodic kernels and, for observers rigidly connected to a helicopter-fixed frame of reference, periodic delays as well (it is worth noting that the periodicity occurs in coordinated turns).

Differently, during unsteady helicopter manoeuvres kinematic and aerodynamic terms are non-periodic, thus increasing the complexity of the algorithms to be applied for implementing Eqs. (1) and (2). Time delays, θ, appearing in thickness and loading noise expressions are obtained as solutions of a root-finding problem for the following nonlinear equation

$$\|\mathbf{x}(t) - \mathbf{y}(t-\theta)\| = c_0\,\theta$$

and thus, the prediction of radiated noise requires the knowledge of the past time histories of blade pressure loads and vehicle and blade kinematics, for a time interval length depending on observer location. Indeed, time histories of center of mass trajectory and velocity, vehicle attitude and angular velocity are necessary data to evaluate instantaneous values of kernels and integral coefficients of the discretized versions of Eqs. (1) and (2).

3.1. Compact-Source Aeroacoustic Formulation

In order to optimize the computational performance of the aeroacoustic solver presented in the previous section, while limiting, at the same time, the amount of data exchange from aerodynamic to aeroacoustic solvers (a particularly relevant issue in noise predictions concerning rotorcraft manoeuvring flights), the so-called compact source versions of it could be conveniently applied. Those introduced in the last decade are based on the knowledge of spanwise distribution of sectional lift;[8, 11] they provide satisfactorily accurate noise predictions when pressure distribution presents limited values of chordwise gradient, and are applicable by using blade loads predicted by aerodynamic models typically considered in rotorcraft comprehensive codes.[12]

Starting from the Farassat 1A Formulation, the compact form of the loading noise term, p'_L, reads[8]

$$(3)\quad 4\pi p'_L(\mathbf{x},t) = \frac{1}{c_0}\int_0^R \left[\frac{\dot{\mathbf{L}}\cdot\hat{\mathbf{r}}}{r|1-M_r|^2}\right]_\tau \mathrm{d}\ell(\mathbf{y}) + \int_0^R \left[\frac{\mathbf{L}\cdot(\hat{\mathbf{r}}-\mathbf{M})}{r^2|1-M_r|^2}\right]_\tau \mathrm{d}\ell(\mathbf{y}) + \frac{1}{c_0}\int_0^R \left[\frac{\mathbf{L}\cdot\hat{\mathbf{r}}\,\left(r\,\dot{\mathbf{M}}\cdot\hat{\mathbf{r}} + c_0 M_r - c_0 M^2\right)}{r^2|1-M_r|^3}\right]_\tau \mathrm{d}\ell(\mathbf{y})$$

where R is the blade radius and, in this case, $\mathbf{r}$ denotes the distance between the observer point, $\mathbf{x}$, and the compacted source point, $\mathbf{y}$, located along the blade span. In addition,

$$\mathbf{L} = -\int_{LE}^{TE} \Delta p\,\mathbf{n}\,\mathrm{d}s$$

is the section force vector, with $\mathbf{n}$ and p denoting upward unit normal to airfoil mean-line and pressure jump, respectively.

The compact-source integral representation in Eq. 3 is applicable when the chord length is negligible with respect to the source-observer distance, r, and predicts the same radiated sound for any chordwise pressure distributions providing the same spanwise distribution of sectional forces, $\mathbf{L}$.

4. AEROMECHANICS AND AERODYNAMICS PREDICTION TOOLS

To support the specific aeromechanics analyses required by the project MANOEUVRES, AgustaWestland makes use of its reference company tools for flight dynamics and aerodynamics simulation: here, these are run in a loosely coupled and modular fashion, to segregate and simplify the solution process and allow parallelization of the technical activities. In practice, first, the fight mechanics software uses a simplified modelling approach for blade dynamics and aerodynamics, to simulate the trimmed conditions, as well as the fully unsteady response of the vehicle, and then, the computed flight parameters are used as inputs to the aerodynamic solver. The aerodynamic simulation is determined by matching the pilot controls, the vehicle flight mechanics states and the main and tail rotor hub generalized forces (and therefore the advance ratio, rotor thrust coefficient, and rotor tip-path-plane angle of attack) as previously calculated in the flight dynamics analysis phase.

4.1. Aeromechanics simulation

Whenever applicable, the flight mechanics simulation of unsteady flight is performed using a manoeuvre tracking technique: similarly to what a pilot would do with the actual vehicle, a set of synthetic autopilot control logics is applied to steer the vehicle virtual model along the desired flight path, either coming from flight tests or designed for the purpose of the prediction task. The autopilot method, well known in the past for helicopter trim simulations, has been effectively applied in past European research efforts (for instance in the software EUROPA used in projects like RESPECT and NICETRIP) and is here implemented in a multi-layer set of generalized control logics, called APHELION.

Note that, as the vehicle considered in the project is a legacy company helicopter with no major configuration changes, the rotorcraft software models employed are extremely accurate and reliable, in that based on past extensive investigations and validations on quite large flight regime envelopes.

One of the key features of the working process described above is that it allows the very efficient use of state-of-the-art methods for each discipline, assuming that the interfaces and the iterations on the computed results are rigorously and transparently defined and performed. For instance, the same flight simulation software, Flightlab® by Advanced Rotorcraft Technology Inc. (ART), can be used in this research in all tasks, from the simple trim calculation to the unsteady simulation of entire flight procedures, or even to piloted simulation trials in the AgustaWestland Engineering Simulator facility. Flightlab® allows users to apply high-fidelity simulation models by arbitrarily selecting from a library of modelling components, interconnecting them into a custom architecture, and assigning aircraft specific data to the parameters of these components.

This flexibility is used here to run the same real-time capable helicopter model with few rotor blade dynamics states, nonlinear compact rotor wake models (Peters-He dynamic wake model), nonlinear modelling of static aerodynamics and flight controls in any flight condition examined, and to connect turboshaft engine, engine control system and flight control system models, for example, only when necessary. Recently, Flightlab® has been one of the main tools applied for the development of the ERICA tiltrotor concept in European research programs like NICETRIP, and is adopted by AW in most of its current design, development and certification activities.

4.2. Aerodynamics simulation

The aerodynamic blade loading required by the acoustic code, is obtained by means of the AgustaWestland in house ADPANEL solver. ADPANEL is a full-unstructured panel code implementing the most advanced aerodynamic features in the field of potential methods. It is capable to represent body surfaces in unstructured-hybrid meshes, while the wake representation is based on the Constant Vorticity Contour (CVC) modelling of both rotary and fixed wing. More in detail, Dirichlet approach was chosen in ADPANEL, since it was found to be more robust and computationally efficient. The wake model implemented in ADPANEL is

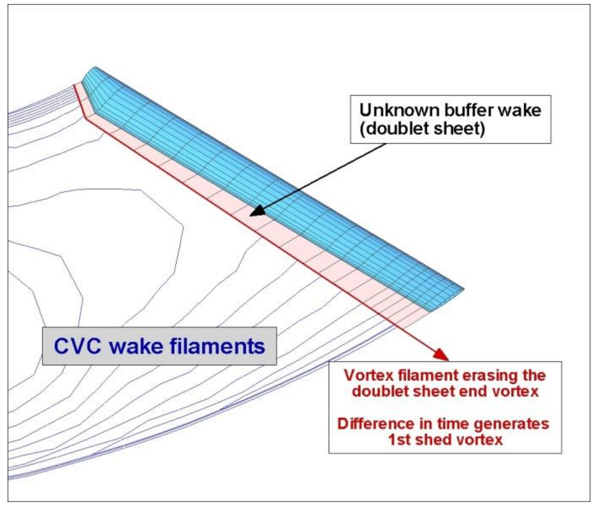

Figure 2: Wake modelling in ADPNEL.

composed by two parts: the dipole buffer wake sheet and a set of Constant Vorticity Contour (CVC) vortex filaments. This dipole is generated every time step and is converted, after the resolution of the Laplace equation, in CVC vortex filaments (see Fig. 2); before the conversion, starting from the second time iteration, an equivalent vortex is generated along the confinement of the buffer region in order to erase the not-balanced amount of circulation while difference in time generates the first shed vortex. Kutta Condition is used to prescribe the stream-wise vorticity released both by wings and rotor blades. Finally a Multi-Block (Iterative) & Accelerated Flow Solver based on a Multi-Processor Implementation (MPI) maximize the ADPANEL computational efficiency.

The peculiarity of its formulation makes ADPANEL suitable to threat complex fully unsteady problems. It provides aerodynamic simulations through a time marching, unsteady solution scheme: suitable input flight parameters are considered for examining simplified problems like, for instance, wings in steady, rectilinear flight.

Within this work, a fully coupled main rotor and tail rotor simulation is applied in order to take into account the interactions between the main rotor wake with the tail rotor blades: based on AgustaWestland experience, this type of aerodynamic simulation is the most reliable for acoustic predictions.

5. SIMPLIFIED AEROMECHANICS MODEL AND NOISE DATABASE APPLICATION FOR STEADY-STATE APPROACHES

In the PAI algorithm for in-flight noise estimation,[6] a simplified flight mechanics model for the helicopter is considered, based on the conservation of linear momentum for a point mass, as expressed by

$$m\,\mathbf{a} = \mathbf{T}_{MR} + \mathbf{T}_{TR} + \mathbf{F} + \mathbf{W}$$

where m is the helicopter gross mass, $\mathbf{a}$ the helicopter center of mass acceleration, $\mathbf{T}_{MR}$ is the thrust vector delivered by the main rotor, $\mathbf{T}_{TR}$ that of the tail rotor, $\mathbf{F}$ the resultant aerodynamic force vector of the fuselage (including empennages), and $\mathbf{W}$ the helicopter gross weight vector. This equation can be recast as

$$\mathbf{T}_{MR} = -\left(\mathbf{T}_{TR} + \mathbf{F} + W\,\mathbf{n}\right)$$

where $W = |\mathbf{W}| = m\,g$ and $\mathbf{n} := \mathbf{W}/g - \mathbf{a}$ is the load factor vector. This allows to evaluate the main rotor thrust coefficient C_T as

$$C_T := \frac{\|\mathbf{T}_{MR}\|}{\rho\,\Omega^2 R^4} = \frac{\|\mathbf{T}_{TR} + \mathbf{F} + W\,\mathbf{n}\|}{\rho\,\Omega^2 R^4}$$

where ρ is air density, Ω is the main rotor speed, and R the main rotor radius. Therefore, by estimating $\mathbf{T}_{TR}$, $\mathbf{F}$ and $\mathbf{n}$, the thrust coefficient is obtained. This implies suitable models for the tail rotor thrust as a function of flight conditions (air density, true airspeed, and fuselage aerodynamic angles, *i.e.,* angle of attack and angle of sideslip) and collective pitch, and for the fuselage aerodynamic resultant, again as a function of flight conditions, while load factor can be directly measured from the on-board inertial unit.

As for advance ratio μ, given its definition as

$$\mu := \frac{V\,\cos\alpha_{TPP}}{\Omega\,R}$$

it depends on true airspeed V and TPP angle od attack, α_{TPP}. The latter characterizes the relative orientation of the airspeed vector with respect to the TPP and, in general, can be evaluated by considering the relative orientation of the airspeed vector with respect to the helicopter fuselage, described by fuselage angles of attack α_F and side-slip β_F composed with the relative orientation of the TPP with respect to the fuselage, described by the cyclic components of the rotor blade flapping angle, *i.e.,* longitudinal flapping, a_{1s}, and lateral flapping, b_{1s}. Considering symmetric flight conditions for the sake of simplicity and a convenient definition of fuselage body axes, the following relation holds:

$$\alpha_{TPP} = \alpha_F + a_{1s}$$

Therefore, the TPP angle of attack can be evaluated by estimating fuselage angle of attack and the main rotor longitudinal flapping.

On this basis, the *technique C* considered here applies the parameters (μ, α_{TPP}) evaluated by the balance of forces discussed above, while the value for C_T is derived from the results of the aeromechanics tool applied to the unsteady manoeuvre, simulating the outcome of an on-board 'ideal' derivation using flight parameters and weight estimates augmented by the measurement of the helicopter acceleration vector via an inertial unit.

Technique B, on the other hand, retrieves the full parameter array (μ, C_T, α_{TPP}) from an algebraic manipulation of the results of the aeromechanics prediction tool. In this way, *technique B* represents what could be achieved from the application of the MANOEUVRES project, where a direct measurement of main rotor blade motion provided by the rotor state measurement system yields an evaluation of longitudinal and lateral flapping angles. This, coupled with a direct measurement (typically, via a swivelling air data boom) or a suitable run-time estimation of fuselage aerodynamic angles, would provide a value for the current TPP angle of attack. In this context, a promising methodology of *observation* of the parameters (C_T, α_{TPP}), which aims to by-pass the need for a separate physical or virtual sensor for the fuselage aerodynamic angles is proposed in Ref. [13].

6. NUMERICAL RESULTS

The acoustic simulation techniques considered in this work are assessed through application to the prediction of noise emitted by the helicopter AgustaWestland AW139 during an approach manoeuvre. The AgustaWestland AW139 is a 15-seat, intermediate-class, twin-engined helicopter, with a 5-blade fully-articulated main rotor of radius $R = 6.9$ m, a 4-blade tail rotor, and maximum take-off weight of 7000 kg.

The unsteady flight examined consists in an approach manoeuvre (named ID8021) starting from a level, steady rectilinear flight at 90 kn, followed by a 40 sec uniform deceleration to 50 kn, a -9 deg slope steady descent flight, and ending with the transition to a final level, steady rectilinear flight. Figures 3-5 depict the evolution of the flight parameters used to parametrize the acoustic database (namely, μ, C_T and α_{TPP}), as determined by the aeromechanics tool to fly the prescribed helicopter manoeuvre (μ is given by manoeuvre specifications). The corresponding flight-path angle, given by manoeuvre specifications, is presented in Fig. 6, whereas Fig. 7 shows the associated main rotor blade pitch controls identified by the aeromechanics tool. In Fig. 5 the TPP-AOA determined by the estimation process applied in *technique C* (see Sections

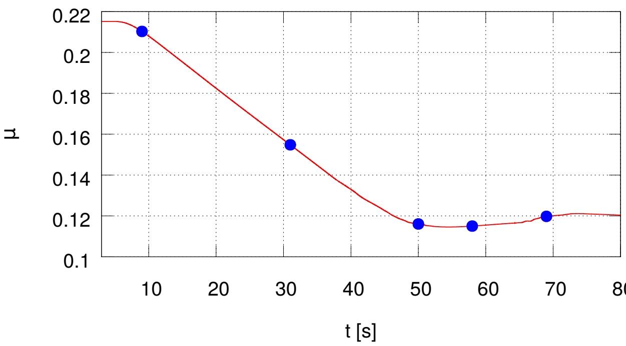

Figure 3: Advance ratio evolution along trajectory.

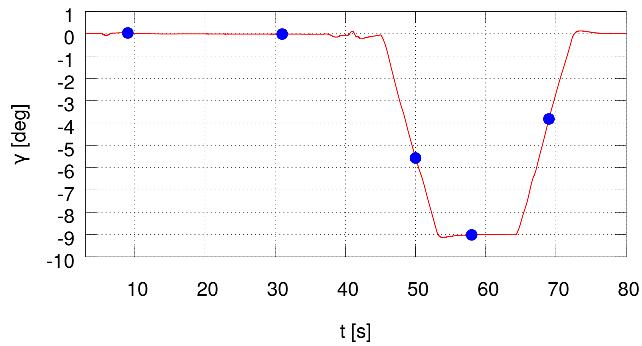

Figure 6: Flight-path angle evolution along trajectory.

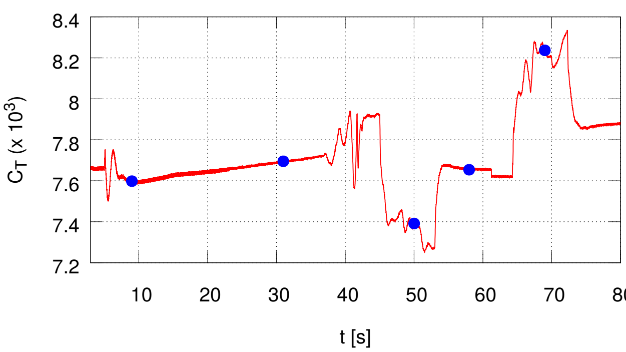

Figure 4: Thrust coefficient evolution along trajectory.

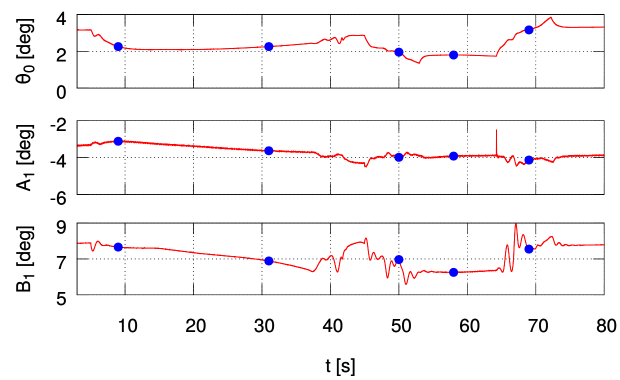

Figure 7: Collective and cyclic controls along trajectory.

2 and 5) is compared to that evaluated by the aeromechanics tool (and used in *technique B*): the discrepancy between the TPP-AOA presented in this figure provides a first assessment of the advantages given by the direct measurement of blade flapping. In each figure, five points along the time histories are marked: these represent flight conditions where different unsteady effects influence the noise emission, and thus seem to be appropriate to assess the capability of the quasi-steady approaches to predict helicopter acoustic disturbance during an arbitrary manoeuvre.

In the first point (at about $t = 9$ sec), the helicopter is at the end of the transition from the steady level flight to the uniformly decelerated flight, with noise affected by unsteady effects mainly through the corresponding α_{TPP} variation (see Fig. 5); in the second point (at about $t = 31$ sec), the helicopter is in uniform decelerated flight, with inertial loads still affecting α_{TPP}; the third point (at about $t = 50$ sec) is located in the middle of the phase of conversion from level to descending flight, where noise is mainly influenced by the unsteady effects due to the trajectory curvature (reduced load factor, see Fig. 4); the fourth point (at about $t = 58$ sec) is in uniform, rectilinear, descending flight, *i.e.,* an operative condition characterized by high sensitivity of the acoustic response to main rotor α_{TPP}; finally, in the fifth point (at about $t = 69$ sec) the helicopter is manoeuvring to restore level flight, and thus the emitted noise is strongly affected by inertial effects on rotor disk loads (increased load factor, see Fig. 4).

In the next sections, the acoustic emissions provided by *technique A* are compared with those estimated by *technique B* and *technique C* on a portion of a sphere of

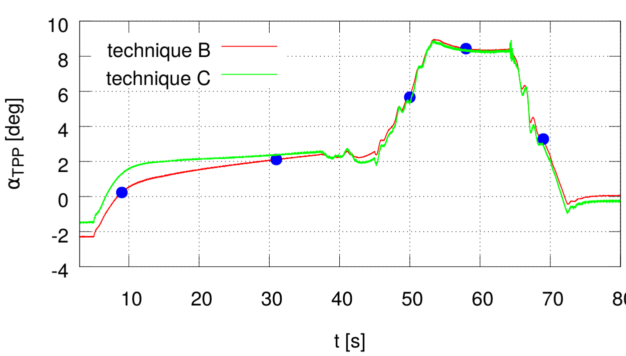

Figure 5: Main rotor tip-path angle evolution along trajectory.

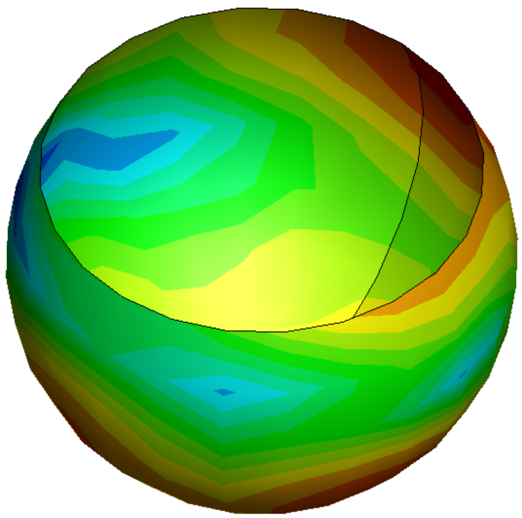

Figure 8: Three-dimensional representation of OASPL evaluated on the hemisphere surface by *technique A* at point 1.

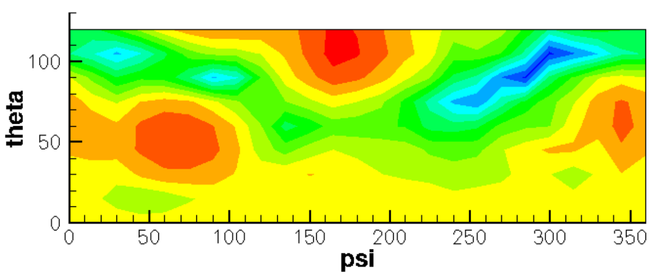

Figure 9: Two-dimensional representation of OASPL evaluated on the hemisphere surface by *technique A* at point 1.

radius $r = 150$ m that surrounds the helicopter, having the equatorial plane parallel to the cabin floor. Specifically, the considered portion of the spherical surface is included in the domain defined by azimuthal angle $\psi = [0, 360]$ and polar angle $\theta = [0, 120]$ (in degrees).

For the sake of clarity, the noise contour plots are provided in the mapped coordinate plane (ψ, θ), with the $\psi = 180$ deg meridian line located forward, $\psi = 90$ deg denoting starboard side, $\theta = 90$ deg representing the equatorial parallel, whereas $\theta = 0$ deg corresponds to the pole located underneath the helicopter. In order to better understand the relation between the distribution of noise on the hemisphere and its two-dimensional representation, Figs. 8 and 9 show the Overall Sound Pressure Level (OASPL) evaluated on the hemisphere at point 1 of the trajectory, respectively through a three-dimensional contour plot view and the corresponding view on the plane (ψ, θ) (the colour scale is such that low-noise regions are in blue, whereas high-noise regions are in red, with a 2 dB colour change step).

6.1. Noise radiated at point 1

For this point, where significant discrepancies between the TPP-AOA value used in *technique B* and that used in *technique C* appear (see Fig. 5), Figs. 10 and 11 show the difference between the OASPL evaluated by *technique A* and those predicted by *technique B* and *technique C* , respectively.

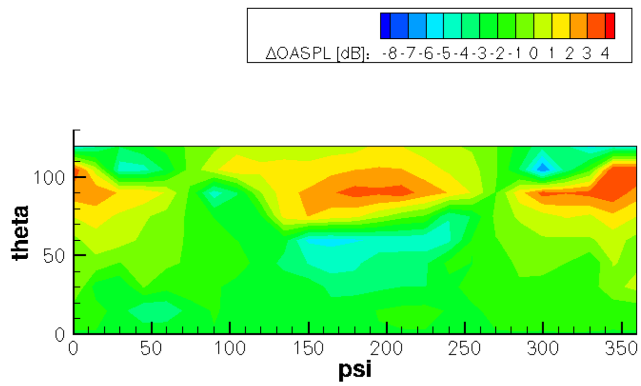

Figure 10: *Technique A-B* differential OASPL at point 1.

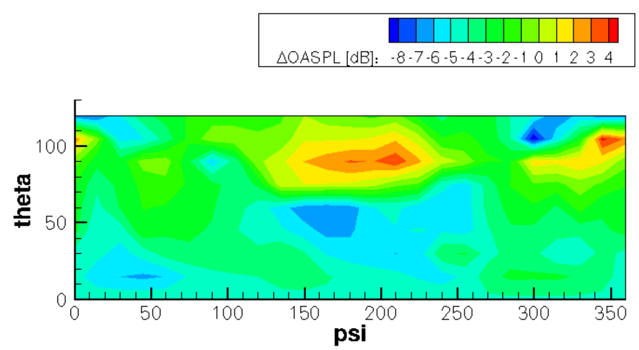

Figure 11: *Technique A-C* differential OASPL at point 1.

First of all, it is possible to observe that both techniques based on the steady-state acoustic database provide a good estimation of the emitted noise on a large portion of the hemisphere, with some underestimation (red areas) or overestimation (blue areas) of the acoustic disturbance appearing in a few regions of limited extension. Furthermore, the comparison of Figs. 10 and 11 reveals that *technique B* predictions are closer than *technique C* ones to those provided by *technique A* (except for a limited hemisphere region across the equatorial circle), thus demonstrating the advantages that are achievable in determining the TPP-AOA from direct rotor state measurements.

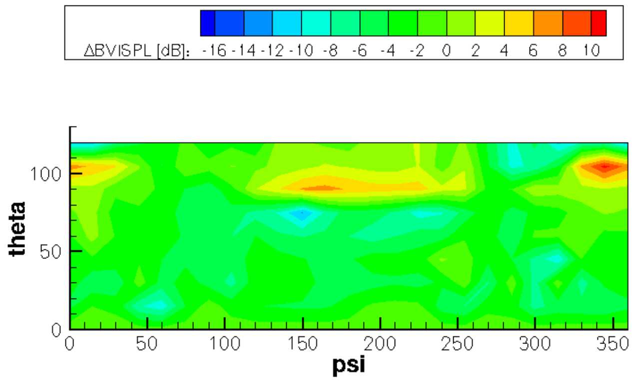

Figure 12: *Technique A-B* differential BVISPL at point 1.

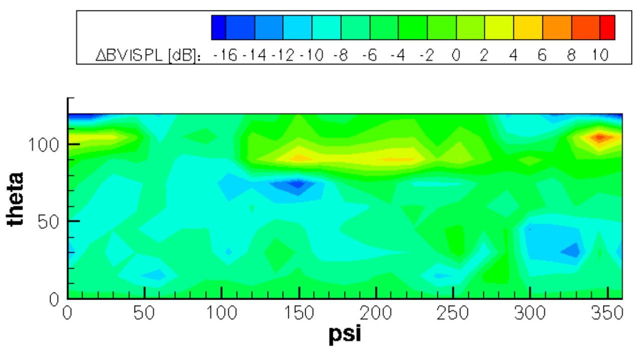

Figure 13: *Technique A-C* differential BVISPL at point 1.

However, more interesting are the comparisons presented in terms of the overall sound pressure level evaluated for the noise frequency range included between the 6-th bpf and the 40-th bpf. Indeed, this noise measure takes into account the most annoying acoustic effects related to blade-vortex interaction phenomena, and for this reason it is commonly named BVISPL. Figures 12 and 13 depict the differential BVISPL contour plots between results given by *technique A* and *technique B* , and *technique A* and *technique C* , respectively. Akin to the OASPL analysis, BVISPL is satisfactorily predicted by quasi-steady approaches at a large part of the examined surface, with significant overestimation and underestimation limited to regions of small area. Likewise, the comparison of the quality of predictions from *technique B* and *technique C* proves the beneficial effects of the availability of accurate estimation of the TPP-AOA, with the former clearly closer to *technique A* simulations, except for a very small area in the equatorial region. This is an important result, in that strictly related with the objectives of the developed PAI device consisting in making the pilot aware of the acoustic annoyance produced by the helicopter manoeuvre.

6.2. Noise radiated at point 2

At this trajectory point the helicopter is in level, rectilinear, uniformly decelerated flight. Unsteady effects are reduced with respect to point 1, and this yields peaks of underestimation/overestimation of BVISPL predicted by *technique B* and *technique C* of lower intensity, as shown in Figs. 14 and 15. Likewise point 1, *technique B* predictions are fairly more accurate than *technique C* ones, particularly in the region below the equatorial zone, which is that more related with the ground radiated noise.

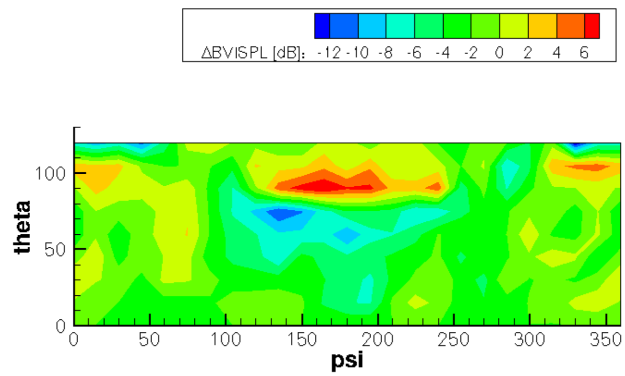

Figure 14: *Technique A-B* differential BVISPL at point 2.

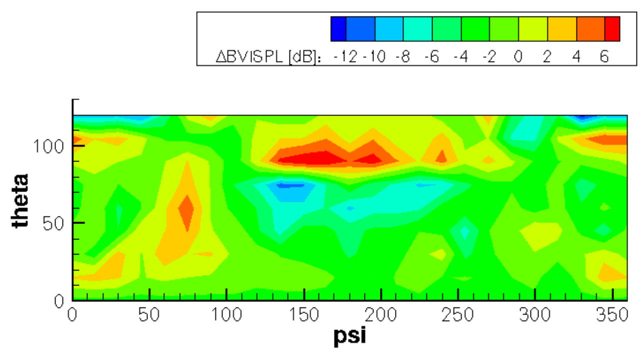

Figure 15: *Technique A-C* differential BVISPL at point 2.

6.3. Noise radiated at point 3

Point 3 is the point of transition from level to descent flight, and from the inertial point of view the dominating effect is the alleviation of the C_T due to the reduction of load factor induced by the curvature of the trajectory. As depicted in Fig. 5, the α_{TPP} in *technique B* and *technique C* is almost identical and, therefore, the noise hemispheres extracted from the database by the two techniques are very similar.The result is that the BVISPL distributions (and OASPL's ones, as well) predicted by *technique B* and *technique C* are very close both in terms of intensity and directivity, as proven by

Figs. 16 and 17 through comparison with *technique A* . Akin to the previous points examined, some overestimation/underestimation of noise is present in the equatorial region.

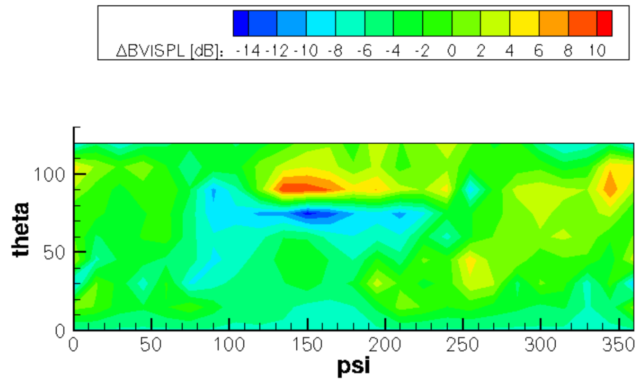

Figure 16: *Technique A-B* differential BVISPL at point 3.

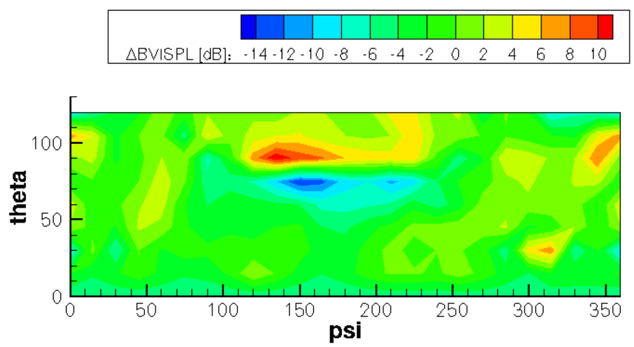

Figure 17: *Technique A-C* differential BVISPL at point 3.

6.4. Noise radiated at point 4

Point 4 is the point where the helicopter is close to a steady operating condition of descending, rectilinear flight (see Figs. 3-6). As expected, *technique A* and *technique B* results are in good agreement (particularly, in terms of the OASPL distribution which tends to hide the small unsteady effects still present at this trajectory point, as shown in Fig. 18) and, as inferred from Fig. 5, *technique C* predictions are very close to *technique B* ones, even in terms of BVISPL (see Fig. 19 that presents the contour plot of the differences between *technique B* and *technique C* outcomes).

6.5. Noise radiated at point 5

At this point, the inertial effects are of the same nature of those at point 3, but of opposite sign, with the trajectory curvature inducing an increase of disk loading. Similarly, acoustic predictions from *technique B* and

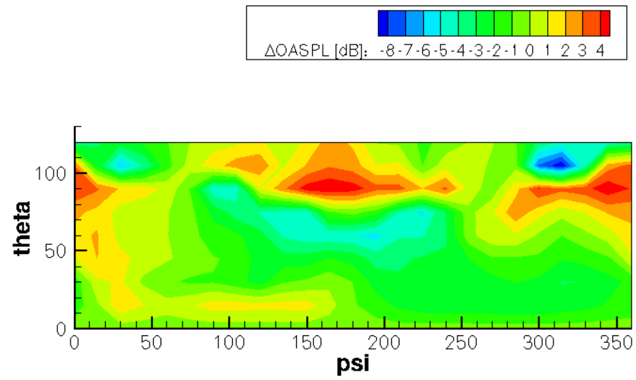

Figure 18: *Technique A-B* differential OASPL at point 4.

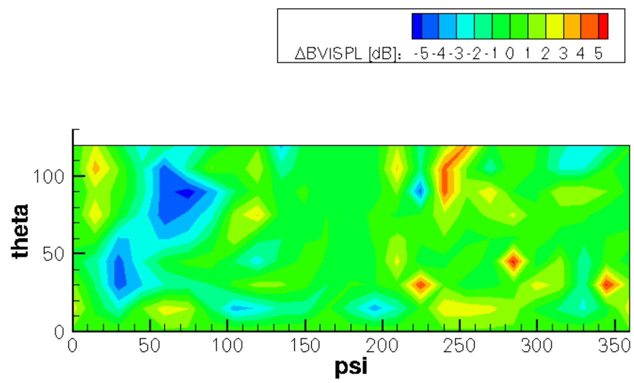

Figure 19: *Technique B-C* differential BVISPL at point 4.

technique C are almost identical and of the same quality of those at point 3. This is an expected outcome, considering that here the influence of inertial effects is much higher on C_T than on α_{TPP}, and observing that α_{TPP} from *technique B* and *technique C* are quite similar (see, Fig. 5). For the sake of conciseness, these results are not shown.

6.6. Noise radiated at point 1 of higher deceleration rate manoeuvres

In view of the aeroacoustic results obtained for the manoeuvre considered, which show that the unsteady effects leading to higher discrepancies between *technique B* and *technique C* predictions are those at point 1, here two additional points of transition from uniform to decelerated flight extracted from different helicopter manoeuvres are examined. Starting from the same level, steady rectilinear flight at 90 kn, both manoeuvres include a a faster deceleration to 50 kn: in the first one it is performed in about 20 s (manoeuvre named ID8022), whereas in the second one the deceleration lasts about 10 s (manoeuvre named ID8023).

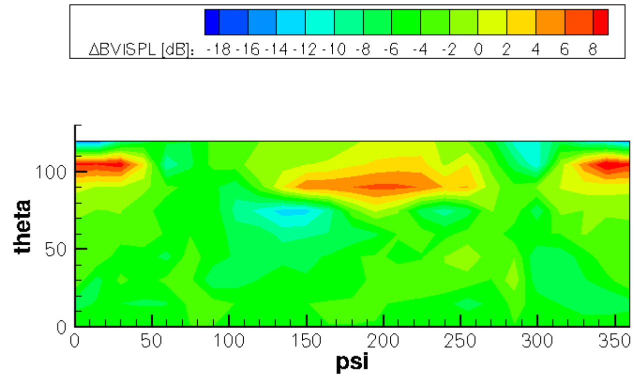

Figure 20: *Technique A-B* differential BVISPL at point 1 of ID8022.

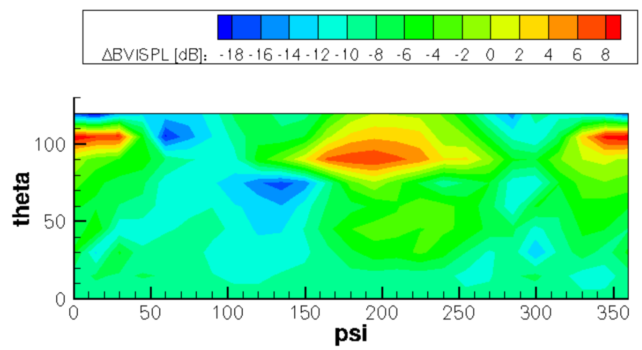

Figure 21: *Technique A-C* differential BVISPL at point 1 of ID8022.

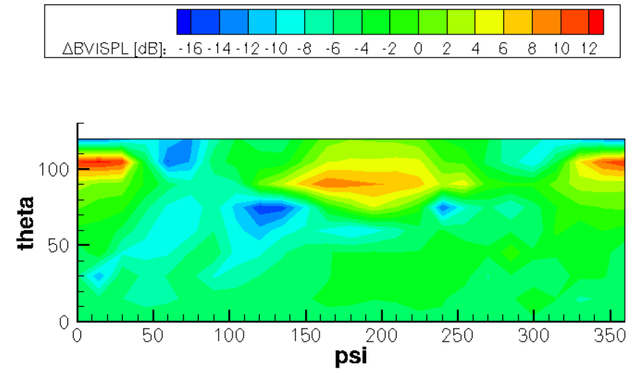

Figure 22: *Technique A-B* differential BVISPL at point 1 of ID8023.

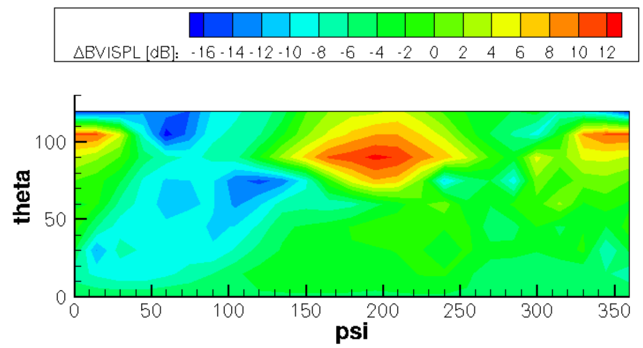

Figure 23: *Technique A-C* differential BVISPL at point 1 of ID8023.

Considering the contour plots of the BVISPL, Fig. 20 shows the differential of predictions from *technique A* and *technique B* , whereas Fig. 21 presents the correlation between *technique A* and *technique C* , for the manoeuvre ID8022. With respect to the basic manoeuvre considered, the prediction provided by *technique B* remains of similar good quality (particularly towards the polar region), whereas *technique C* presents areas of larger discrepancy as compared with *technique A* .

Similar considerations may be drawn observing Figs. 22 and 23, that concern the correlations of *technique B* and *technique C* with *technique A* for the first point of manoeuvre ID8023, where higher unsteady effects arise. Small isolated regions of high underprediction/overprediction of the acoustic signal appear, but tend to be confined in the equatorial region. Nonetheless, *technique B* results remain of good quality soon below the equatorial circle, thus confirming the suitability of *technique B* for application within the PAI system. In addition, the improvement in noise prediction quality moving from *technique C* to *technique B* is increased with respect to what observed at point 1 of trajectories ID8021 and ID8022.

7. CONCLUSIONS

Two quasi-steady noise prediction techniques (*technique B* and *technique C*) based on the availability of a database of steady-flight noise simulations have been developed, successfully applied to manoeuvring flights and compared with solutions provided by an unsteady aeroacoustics solver (*technique A*). One (*technique B*) takes advantage of TPP-AOA measurements, whereas the other (*technique C*) relies on a numerical estimation of the TPP-AOA. ¿From the comparison of noise predicted by *technique B* and *technique C* with that provided by *technique A* for an arbitrary unsteady approach manoeuvre of the AW139 helicopter, the following conclusions may be drawn:

– as expected, the lower the manoeuvre unsteady effects, the closer *technique B* and *technique C* predictions to *technique A* ones;

– as expected, OASPL quasi-steady predictions are more accurate than BVISPL ones;

– as expected, the quasi-steady techniques provide very similar results at those trajectory points where manoeuvring unsteady effects are either negligible or scarcely influence the TPP-AOA;

- the weakest point of *technique B* and *technique C* predictions is the simulation of noise at the level of the rotor plane; better quality is observed beneath it, *i.e.,* in the region more strictly related to ground radiated noise;
- except for small extent areas around the hemisphere equatorial region, *technique B* predictions are definitely closer than *technique C* predictions to *technique A* simulations, thus demonstrating the advantages deriving from direct measurements of the TPP-AOA;
- the difference of prediction accuracy between *technique B* and *technique C* grows with the increase of manoeuvre unsteady effects.

The numerical investigation has been carried out considering only the noise emitted by the main rotor: further activity for the project MANOEUVRES will consists both in extending the analysis to the main rotor/tail rotor system, and in investigating additional quasi-steady techniques more realistically including the on-board numerical estimation of the main rotor thrust coefficient.

ACKNOWLEDGMENTS

The research leading to these results has received funding from Project MANOEUVRES, financed by European Community's Clean Sky Joint Undertaking Programme under Grant Agreement N. 620068.

REFERENCES

[1] D.A. Conner, J.A. Page, "A Tool for Low Noise Procedures Design and Community Noise Impact Assessment: The Rotorcraft Noise Model (RNM)," Proceedings of Heli Japan 2002, Tochigi, Japan, 2002.

[2] A. Le Duc, P. Spiegel, F. Guntzer, M. Kummer, J. Götz, "Modelling of Helicopter Noise in Arbitrary Maneuver Flight Using Aeroacoustic Database," Proceedings of the 9th Onera-DLR Aerospace Symposium (ODAS 2008), Châtillon, France, 2008.

[3] S. Hartjes, Y. Buys, H.D. Visser, M.D. Pavel, M. Gennaretti, G. Bernardini, M. Arntzen, "Optimization of Rotorcraft Noise Abatement Trajectories," Proceedings of Internoise 2012/ASME NCAD meeting, New York City, USA, 2012.

[4] L. Trainelli, A. Rolando, E. Zappa, S. Manzoni, M. Lovera, M. Gennaretti, G. Bernardini, P. Cordisco, M. Terraneo, E. Vigoni, R. Grassetti, "MANOEUVRES An Effort Towards Quieter, Reliable Rotorcraft Terminal Procedures," Proceedings of Greener Aviation: Clean Sky breakthroughs and worldwide status, Brussels, Belgium, pp 1-7, 2014.

[5] L. Trainelli, M. Lovera, A. Rolando, E. Zappa, M. Gennaretti, P. Cordisco, R. Grassetti, M. Redaelli, "Project MANOEUVRES Towards Real-Time Noise Monitoring and Enhanced Rotorcraft Handling Based on Rotor State Measurements," Proceedings of the 41st European Rotorcraft Forum, Munich, Germany, 2015.

[6] A. Rolando, F. Rossi, C. E. D. Riboldi, L. Trainelli, R. Grassetti, D. Leonello, M. Redaelli, "The Pilot Acoustic Indicator: A Novel Cockpit Instrument for the Greener Helicopter Pilot," Proceedings of the 41st European Rotorcraft Forum, Munich, Germany, 2015.

[7] A. D'Andrea, "Development of a Multi-Processor Unstructured Panel Code Coupled with a CVC Free Wake Model for Advanced Analyses of Rotorcrafts and Tiltrotors,"Proceedings of the American Helicopter Society 64th Annual Forum, Montréal, Canada, 2008.

[8] K.S. Brentner, H.E. Jones, "Noise Prediction for Maneuvering Rotorcraft," AIAA Paper 20002031, Proceedings of the 6th AIAA/CEAS Aeroacoustics Conference, Lahaina, Hawaii, 2000.

[9] F. Farassat, "Derivation of Formulations 1 and 1A of Farassat," NASA TM 214853, 2007.

[10] J.E. Ffowcs Williams, D.L. Hawkings, "Sound Generation by Turbulence and Surface in Arbitrary Motion," *Philosophical Transactions of the Royal Society*, London, Series A, Vol. 264, No. 1151, pp. 321-342, 1969.

[11] G.A. Brès, K.S. Brentner, "Maneuvering Rotorcraft Noise Prediction," *Journal of Sound and Vibration*, Vol. 275, 2004, pp. 719-738.

[12] W. Johnson, "Comprehensive Analytical Model of Rotorcraft Aerodynamics and Dynamics," Vol. I - VII, Johnson Aeronautics, September 1998.

[13] L. Trainelli, C.E.D. Riboldi, M. Bucari, "Observing the Angle of Attack of the Tip-Path Plane from Rotor Blade Measurements," Proceedings of the 41st European Rotorcraft Forum, Munich, Germany, 2015.